

Numerical and workbench design of 2.35 T double-tuned ($^1\text{H}/^{23}\text{Na}$) nested RF birdcage coils suitable for animal size MRI

Marco Fantasia, Angelo Galante, Francesca Maggiorelli, Alessandra Retico, Nunzia Fontana, Agostino Monorchio and Marcello Alecci*

Abstract— The birdcage Radio Frequency (RF) coil is one of the most used configurations in Magnetic Resonance Imaging (MRI) scanners for the detection of the proton (^1H) signal over a large homogeneous volume. More recently, birdcage RF coils have been successfully used also in the field of X-nuclei MRI, where the signal of a second nucleus (e.g. ^{13}C , ^{23}Na , ^{31}P , and many others) needs to be detected with high sensitivity and spatial homogeneity. To this purpose several technical solutions have been adopted to design Double Tuned (DT) volume RF coils, including the recent configuration of the nested birdcage RF coils. One of the main problems in the design of DT RF coils is the decoupling between the ^1H and X channels, and a number of solutions have been adopted over the years. In this work, based on numerical and workbench methods, we report the decoupling optimization of DT ($^1\text{H}/^{23}\text{Na}$) nested RF birdcage coils suitable for 2.35 T MRI scanners encompassing an inner Low-Pass (LP) birdcage used for X-nuclei, an outer High-Pass (HP) birdcage for ^1H and an external cylindrical RF shield. We show that a suitable geometrical selection of the two coaxial RF birdcage coils (relative angular orientation, diameters and lengths) and RF shield (diameter, length) allows a significant decoupling optimization. We also provide valuable information about the RF B_1^+ field homogeneity and efficiency. Our approach was validated both with numerical simulations and workbench testing using DT nested RF coil prototypes.

Index Terms—MRI, RF coil, birdcage, double tuned, nested, decoupling.

I. INTRODUCTION

THE development of ultra-high-field (≥ 3 T) Magnetic Resonance Imaging (MRI) is driving an increasing interest for the detection of X-nuclei (e.g. ^{13}C , ^{23}Na , ^{31}P , and many others) [1-2] that play an important role in biological systems. The utility of X-nuclei MRI and spectroscopy is enhanced, for assessing normal physiology, diseases and therapeutic responses, when it is paired with co-registered anatomical proton (^1H) images. The best outcome is achieved when anatomical (^1H) and physiological (X-nucleus) images are acquired simultaneously or subsequently using a DT RF coil [3]. This avoids sample re-positioning problems occurring

using separate RF coils in subsequent acquisition scans [4] but introduces some degree of signal losses in the X-nuclei channel. A recent design of DT RF coils proposed the use of PIN-diode switches at 9.4 T [5-6].

Over the years, many surface, volume and array DT RF coil designs have been described in the literature. Surface [3, 7-11] and array [12-13] DT RF coils present high sensitivity (and hence improved Signal-to-Noise Ratio, SNR) in sample regions close to the surface of the RF coil element but shows poor RF B_1^+ spatial homogeneity. As for single tuned RF coils, volume DT RF coils [14-30] have the advantage of a more homogeneous RF B_1^+ spatial distribution as compared to surface DT RF coils, ensuring imaging of the whole sample without image intensity artifacts, albeit with a lower SNR than surface RF coils. In general, when a homogeneous RF B_1^+ spatial distribution is paramount, the use of a transmit-only volume DT RF coil is necessary to ensure the same flip angle in the entire Field of View (FOV), while for signal detection either a surface, an array or a volume DT RF coil can be used.

Among the variety of volume RF coils proposed over the past three decades, the birdcage RF coil is one of the most used because of: (i) its circularly symmetric structure which, in turn, allows to achieve excellent RF B_1^+ field homogeneity; (ii) its ability to be driven in circular polarization modality, increasing the SNR; and (iii) its easy manufacturing process. Due to its versatility the birdcage RF coil is used in many laboratories and represents the first option to be considered for ^1H and X-nuclei applications.

To this purpose, several DT birdcage RF coil designs have been described in literature [14-16, 18-20, 24-30]. One approach is based on the alternate tuning, at the two desired frequencies, of the N legs comprising the coil structure [18-19, 27]. In this case trap circuits have to be inserted in the N/2 legs tuned at the lower frequency for X-nuclei detection. The main drawbacks are a complex tuning procedure, some difficulty in realizing circular symmetry (because of the lumped elements tolerances), and a significant degradation of the RF coil quality factor (Q).

We are grateful to the INFN grant “NextMR 2015-2018”. (M. Fantasia and A. Galante are co-first authors). (* Corresponding author: M. Alecci).

M. Fantasia is with the Department of Life, Health and Environmental Sciences, University of L'Aquila, L'Aquila, Italy (e-mail: marco.fantasia@aquila.infn.it). A. Galante and M. Alecci are with the Department of Life, Health and Environmental Sciences, University of L'Aquila, L'Aquila, Italy; Istituto Nazionale di Fisica Nucleare (INFN), Laboratori Nazionali del Gran Sasso, Assergi, L'Aquila, Italy; and CNR-SPIN, Department of Physical and Chemical Sciences, L'Aquila, Italy (e-mail: angelo.galante@univaq.it, marcello.alecci@univaq.it).

F. Maggiorelli is with the Department of Physical Sciences, Earth and Environment, University of Siena, Siena, Italy and Istituto Nazionale di Fisica

Nucleare (INFN, Sez. Pisa), Pisa, Italy (e-mail: francesca.maggiorelli@pi.infn.it).

A. Retico is with the Istituto Nazionale di Fisica Nucleare (INFN, Sez. Pisa), Pisa, Italy (e-mail: alessandra.retico@pi.infn.it).

N. Fontana is with the Consorzio Nazionale Interuniversitario per le Telecomunicazioni (CNIT), Pisa, Italy (e-mail: nunzia.fontana@cnit.it).

A. Monorchio, is with the Department of Information Engineering, University of Pisa, Pisa, Italy (e-mail: agostino.monorchio@unipi.it).

An alternative solution is the four-ring birdcage RF coil, with a LP birdcage positioned, along the coil axial direction, in between two HP birdcages, the latter sharing the inner end-rings with the former [16]. This solution, although elegant, could give a reduced RF coil efficiency for the ^1H channel due to the increased distance among the external HP structures, a reduced access to the sample (head and shoulders) along the coil longitudinal axis and the presence of unwanted coupling among resonant modes when the sample is not symmetric along the axial direction. Recently, a folded version of the DT four-ring birdcage RF coils has been described [30] with the aim to reduce sample length restrictions.

Another design described in the literature is based on the use of two nested coaxial birdcages, including an inner LP used for X-nuclei, an outer HP for ^1H and an external cylindrical RF shield [24-27, 29]. In the original paper [24] introducing the nested DT birdcage design, with both X-nuclei and ^1H operating on both channels in quadrature, it was already noted that the performance of the X-nuclei channel is near ideal, while the ^1H useful mode suffers from a relatively large degree of inefficiency due to counter-rotating currents flowing in the other birdcage. Moreover, it was also already noted [24] that due to this residual coupling, the ^1H RF field spatial homogeneity is strongly affected with respect to the isolated ^1H birdcage design. This solution, simpler to manufacture, is considered the first option for a do-it-yourself approach, retaining many advantages of the single-tuned birdcage RF coil: construction simplicity, excellent RF field homogeneity over a large FOV, high Q, and good RF efficiency. However, so far, a full methodological study related to the quantitative optimization of the decoupling between the ^1H and X-nuclei channels of the nested DT birdcage RF coil has not been reported. This coupling is a relevant feature to be considered because significantly shifts the resonant frequencies of the two birdcages with respect to the isolated condition, making the design process cumbersome, and reducing sensitivity. As reported in [24] it was noticed that in the nested DT coil the frequency shift due to mutual coupling is relatively small and negative for the X-nuclei, and positive and larger for the ^1H channel, as predicted within the framework of transformer coupled resonant circuits [24; 31]. In the literature it was only reported, without theoretical and/or experimental evidence, that coupling is reduced by positioning the legs of the inner LP midway between the legs of the outer HP [25].

In this work, based on numerical and workbench methods, we report the decoupling optimization of DT nested RF birdcage coils suitable for MRI scanners. The optimized design, validated at 2.35 T, is based on the use of an inner LP for ^{23}Na (26.5 MHz), an outer HP for ^1H (100.3 MHz) and an external cylindrical RF shield. We show that a suitable geometrical design (birdcages relative angular orientation, diameters and lengths; RF shield diameter and length) allows a significant reduction of the coupling, which simplifies the tuning procedure. We also provide valuable information about the RF B_1 field homogeneity and efficiency. Our approach was validated both with numerical simulations and workbench testing on DT nested prototypes.

A. Finite Element Method (FEM) Simulations

FEM is a fundamental computational tool for RF coils prototyping [32]. We used Ansys Electronics Desktop v. 17.2 (previously known as HFSS) running on a PC with an i7 processor (3.5 GHz) and 32 GB of RAM in both Eigenmode and Modal Network Analysis (MNA) modalities. The former can be used for eigenfrequency analysis (resonant modes frequencies and corresponding electromagnetic field distributions) without the need of port insertion, thus preserving the intrinsic symmetry of the RF coil. The latter requires the insertion of one or more ports and is designed for frequency domain analysis, providing scattering parameters (S-matrix elements) and electromagnetic field distributions at any desired frequency. A minimum of 2×10^5 tetrahedra elements were considered in the integration region, while the convergence criteria, defined as maximum change between the last three successive iterations, was at least 0.2 % for the Eigenmode resonant mode frequencies and 0.01 for the MNA maximum variation in the S-matrix elements. The Eigenmode simulation takes about 20 min for the single birdcage and about 30 min for the nested DT configuration. The MNA simulation requires approximately 50 % less CPU time.

Other methods based on the 3D EM and RF circuit co-simulation have been described allowing the fast analysis of multi-element MRI coils [33].

B. FEM Models and Coupling Calculation

The $^1\text{H}/^{23}\text{Na}$ nuclei combination has been previously used for several MRI studies of stroke, ischemia, articular cartilage, osteoarthritis, transplanted kidney, and cancer, both in animal models and humans [34-42].

When using the nested DT design, in principle, there are four possible configurations for the X-nucleus and the ^1H RF coil birdcages, respectively: LP-LP; LP-HP; HP-LP; HP-HP. To minimize coupling, the two regions of high electric-field (middle plane for the LP birdcage; endrings for the HP birdcage) have to be quite far apart from each other [24, 43]. This restricts the choice to the LP-HP and HP-LP configurations, with the LP-HP usually preferred making easier the tuning of the useful resonant modes for both the X-nuclei and ^1H birdcage coils in a wide range of magnetic fields.

We considered a transceiver system composed by: (i) an inner LP for ^{23}Na with 8 legs, length L_{LP} and diameter D_{LP} ; (ii) a larger HP for ^1H with 8 legs, length L_{HP} and diameter D_{HP} ; and (iii) an external RF shield with diameter D_s and length L_s . Whereas the width of legs and end-rings is fixed to 5 mm, and the thickness of copper strip to 35 μm , several values are considered for L_{LP} , D_{LP} , L_{HP} , D_{HP} , D_s and L_s . The inner position of the LP was chosen to maximize the intrinsic lower SNR from the ^{23}Na nuclei in biological tissues. The considered dimensions are suitable for preclinical MRI studies with whole rats.

To study the dependence of coupling between the ^1H and ^{23}Na channels from the geometrical configurations we used the following FEM models (see Fig. 1):

1) Variation of the LP rungs angular position (θ) with respect to the HP ones for $0^\circ \leq \theta \leq 45^\circ$, using a step size $\Delta\theta = 3.75^\circ$. Fixed HP size ($D_{\text{HP}} = 105$ mm, $L_{\text{HP}} = 160$ mm) and different lengths of the LP ($D_{\text{LP}} = 90$ mm, $L_{\text{LP}}/L_{\text{HP}} = 6, 4, 3, 2, 1.67, 1.34, 1, 0.81, 0.65, 0.50$). Figure 1 shows the LP configurations corresponding to the “long length LP_L” (130 mm), “middle length LP_M” (104 mm) and “short length LP_S” (80 mm).

2) Fixed LP size ($D_{\text{LP}} = 90$ mm, $L_{\text{LP}} = 104$ mm) and different diameters of the HP ($L_{\text{HP}} = 160$ mm, $D_{\text{LP}}/D_{\text{HP}} = 0.25, 0.50, 0.70, 0.86, 0.93$).

3) Fixed HP size ($D_{\text{HP}} = 105$ mm, $L_{\text{HP}} = 160$ mm), with RF shield of different lengths ($L_{\text{S}}/L_{\text{HP}} = 2.00, 1.62, 1.31, 1.00, 0.65, 0.43, 0.22$) and diameters ($D_{\text{S}}/D_{\text{HP}} = 1.58, 1.43, 1.29, 1.14$), to address the perturbation of coupling due to the introduction of the RF shield.

In the nested DT birdcage RF coil the coupling between the two birdcages is responsible for the modes' frequency repulsion, giving a frequency shift (Δf) with respect to the isolated birdcage RF coils. The frequency shift depends on both the degree of coupling and the intrinsic losses of the nested RF coils. Thus, in general it is not possible to convert the degree of coupling from the measured frequency shift alone. For this reason, the frequency shift parameter is commonly used by the designers to fine tune the DT coils [43].

In the following we quantify only the frequency shift of the useful MRI modes of the nested birdcages. For small interaction, the shift is proportional to the original frequency: a larger (and positive) value for the higher HP; a smaller and negative value for the LP [44-46]. Since the $\Delta f/f$ of the LP is less than 1 % for the whole range of design conditions, our whole data set focuses on the HP response alone. Thus, the HP frequency shift is the most sensitive parameter to estimate the

coupling and it was computed by means of the Eigenmode FEM simulations. The evaluation of the frequency shifts provides valuable information about mutual coupling in a nested DT birdcage coil, and this in turn is useful to optimize the tuning procedure.

The isolated birdcages were first tuned by means of: 8 identical capacitors inserted in each end-ring of the HP; 2 identical capacitors inserted in series within each leg of the LP (each capacitor positioned at one third of the leg length, such to reduce the electric field in the central section of the RF coil). Since results are based on the frequency shift calculation, no efforts were made to fine-tune the resonant frequencies of the isolated birdcages, which were very close (within 1%), but not necessarily coincident, to the ^1H and ^{23}Na resonances at 2.35 T.

The effect of loading was comprised in the FEM simulations by means of a short (length 80 mm) and long (210 mm) cylindrical (diameter 59 mm) phantoms containing physiological saline ($\epsilon_r = 78$; $\sigma = 1.67$ S/m).

C. FEM Simulations of RF Field Homogeneity and Efficiency

The numerical FEM simulations were used for the quantitative evaluation of the RF B_1 field profiles and RF coil efficiency. To this purpose, the field profile was calculated along the RF coil symmetry axes (longitudinal and radial directions) crossing the isocenter. The RF field profile (Eigenmode simulation) was normalized to its value at the isocenter, for a better comparison of spatial homogeneity. When comparing the absolute B_1 field results from different geometrical configurations we discovered unreliable results in the Eigenmode simulation outputs. We concluded that, while the normalized RF field profiles were useful, the absolute intensity values provided by the Eigenmode modality are not, thus preventing a fair comparison among different simulation runs.

To assess the RF coil efficiency, defined as B_1^+ field amplitude (T) produced by 1 W driving input power in matched condition, we used the MNA tool by inserting at least one driving port (output impedance 50Ω) connected in parallel to a birdcage tuning capacitor through a suitable impedance matching circuit. In the MNA simulations, we adopted linear driving of each RF birdcage coil. In this condition the birdcage, as seen from the port, behaves as an equivalent parallel LC resonator, with diverging real part of the impedance at the characteristic resonant frequency. After the identification of the useful resonant peak, we determined the unique frequency value f_0 such that, close to the resonant frequency, $Re[Z(f_0)] = 50 \Omega$ and $Im[Z(f_0)] > 0 \Omega$. The RF coil matching was achieved by inserting a single lumped capacitor $C_M = 1/\{2\pi f_0 Im[Z(f_0)]\}$ in series with the port, such as to compensate the inductive reactance at f_0 . The MNA simulation is iterated to achieve an optimal matching condition of at least $S_{11}(f_0) = -25$ dB. In this condition, the absolute RF B_1 field at the coil isocenter (power input of 1 W on the port) was used to quantify the RF coil efficiency. Clearly, a small change of the tuning frequency (less than 2 %) appears after the insertion of the matching capacitor

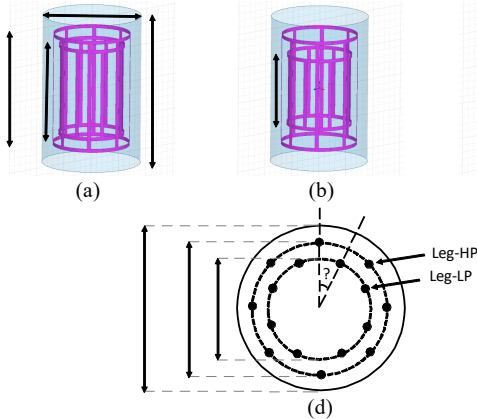


Fig. 1. (a)-(b)-(c) Geometrical configurations of the double-tuned (DT) nested RF birdcage coil considered in the FEM modeling and made by a Low Pass (LP) birdcage RF coil, a High Pass (HP) birdcage RF coil, and a cylindrical RF shield. Simulated sizes are reported in section II.B. The LP lengths $L_{\text{LP}} = 130, 104, 80$ mm are shown in the pictures and referred as “long”, “middle” and “short”. (d) Central transverse cross section of the DT nested RF birdcage coil showing the relative angle θ and diameters between the LP and HP coils.

C_M . The RF coil can be fine-tuned with an iterative procedure to the exact desired frequency. We checked that the fine-tuning procedure gives a non-detectable effect on the RF B_1^+ field numerical results. The above procedure can be applied both in the unloaded and loaded condition.

FEM simulations included the following steps: first, the HP coil, both isolated and in the presence of the RF shield, was tuned and matched, and the RF fields (E , B_1^+) distributions calculated; then, the LP coil (tuned but without driving port) was inserted, the HP coil was re-matched, and the perturbed RF fields calculated. The same procedure was followed to study the effect of the HP coil inserted around the LP coil.

D. Workbench Testing of the $^1\text{H}/^{23}\text{Na}$ Birdcage RF Coil



Fig. 2. Nested DT RF birdcage coil prototypes suitable for 2.35 T applications (geometrical details in section II.D). Left to right: short and long samples; short and long ^{23}Na LP; ^1H HP; and RF shield. The coupling loop is also shown.

The nested DT RF coil prototypes used for workbench testing were dimensioned such as to be suitable for whole rat MRI at 2.35 T, i.e. insertion diameter of about 7 cm and useful FOV along the longitudinal direction of at least 5 cm (Fig. 2). For practical reasons, few of the actual physical dimensions were slightly different from the one used in the FEM simulations. The first prototype is composed by: a long L_{LP} for ^{23}Na (8 legs, length 130 mm, 75 mm diameter, 6 mm width of legs and end-rings, 35 μm copper strips thickness) tuned to about 27 MHz; a HP for ^1H (8 legs, 160 mm length, 100 mm diameter, 13 mm width of legs and end-rings, 35 μm copper strips thickness) tuned to about 100 MHz; and an external RF shield (140 mm diameter, 210 mm length, 100 μm copper thickness). A second shorter (length 80 mm) L_{PS} prototype suitable for ^{23}Na workbench testing was also made for comparison with the theoretical FEM models. PVC mechanical forms (thickness 2 mm) were used for positioning the RF coils and the shield. The tuning capacitors for the HP, long LP and short LP RF coils are 47 pF, 470 pF and 690 pF, respectively. Balanced inductive coupling loops of 4 cm diameter were used to drive and critically match (at least -15 dB) the RF coils [46]. In order to obtain optimal power transfer to the RF coil it is necessary to match the input impedance to the transmission line impedance and the input reactance to zero at the resonant frequency. In our experimental setup we choose the inductive loop matching system because of its practical advantages when designing and testing a large set of DT nested RF coils. Other matching

circuits, including balanced capacitive networks are described in the literature [46] and could be adopted as well. A Network Analyzer (Rhode&Swartz, ZVL3) allowed measuring the S_{11} parameter and the resonant frequency of the prototypes in geometrical conditions corresponding to the FEM models: (i) isolated birdcages without and with the RF shield; (ii) variable azimuthal angle between the LP and HP legs; and (iii) the above configurations with loading phantoms.

The discrete azimuthal rotational symmetry of the LP and HP birdcage legs reduces the independent angular positions to the interval $[0^\circ, 22.5^\circ]$. Nevertheless, we extended the measuring range to $[0^\circ, 45^\circ]$, considering 5 equally angular sampling points. The first and last angular positions correspond to the legs of the HP and LP perfectly superimposed. The extended measurement range interval allows to check the expected resonators symmetry with respect to the central value, $\theta = 22.5^\circ$.

III. RESULTS

A. FEM Simulations for Coupling Determination

Figure 3a summarizes the $\Delta f/f$ frequency shift derived from the Eigenmode FEM simulations for the nested DT birdcage RF coil comprising the long LP and the HP birdcage coil ($L_{LP}/L_{HP} = 0.81$) without and with RF shield ($L_S/L_{HP} = 1.31$) of various diameters versus the relative azimuthal angular position. Due to the RF coils symmetry and the absence of driving ports an even function describing the frequency shift in the $\theta = [0, 45^\circ]$ range is expected. We observe that without RF shield the frequency shift ranges from about 21 to 16 % as the azimuthal angle is adjusted in the full range, with the minimum value observed at $\theta = 22.5^\circ$, a result in agreement with previous qualitative studies [25, 26]. We interpret this as corresponding to the condition of minimal magnetic flux linkage between the two RF birdcage coils. The residual asymmetry, with respect to the central angular value, of the observed $\Delta f/f$ in Fig. 3a gives an estimate of the numerical accuracy of the FEM results. Surprisingly, the insertion of the RF shield significantly reduces the frequency shift, while leaving the minimum at the critical angle of 22.5° . It can be seen that the frequency shift at the critical angle decreases from about 8 % to 1 % when D_S/D_{HP} is reduced from 1.58 to 1.14. Similar results, shown in Figs. 3b and 3c, were obtained with two shorter LP RF coil models. We observe that the value of the shifts is significantly reduced for shorter LP coils, e.g. without shield the shift is reduced from about 16 % to 7 % as the LP coil length is reduced from about 81 % to 50 % of the length of the HP coil.

These findings suggest that, assuming a given geometry (diameter and length) for the LP and HP birdcage RF coils associated to the specific application, the mutual orientation at the critical angle of 22.5° and the presence of a RF shield having an appropriate diameter and length with respect to the HP birdcage coil, allow to minimize the frequency shift of the HP coil in the nested condition. In our specific geometry we observed a significant reduction, and in some case a nulling (within the numerical accuracy of the simulations estimated

below 1%), of the frequency shift for $D_S/D_{HP} \leq 1.29$ (Fig. 3b and 3c).

To better understand the relevance of the contribution of the end-rings of the LP ($D_{LP} = 90$ mm) and HP ($D_{HP} = 105$ mm) birdcages, the $\Delta f/f$ was calculated, without RF shield and for $\theta = 22.5^\circ$, considering an HP coil of fixed length (160 mm) and an LP coil of variable length (from 0, corresponding to the HP alone, to $6 \cdot L_{HP}$). The results, reported in Fig. 4a, show that the frequency shift has a maximum of about 22 % for $L_{LP}/L_{HP} = 1$, a condition corresponding to the closest position between the end-rings. As $L_{LP} > 3 \cdot L_{HP}$ the frequency shift is reduced to a much smaller value. In this condition the end-ring coupling can be considered negligible and the residual frequency shift (about 2 %) can be associated to the legs mutual coupling only. It is worth noting that Fig. 4 (a) reports ratios of the length of the LP coils up to six times that of the HP one. Although this condition of long LP with respect HP has shown some practical applications [43], we are interested in the more commonly used configuration of LP shorter than HP, useful to maximize low gamma SNR. Since we are interested in estimating the legs residual coupling in the nested DT coil, in Fig. 4 (a) we reported also the 1H % frequency shift for LP/HP length ratio larger than 2 to reduce the end-ring coupling contribution at a negligible level. We observe that in this condition the residual frequency shift is about 2 %.

Figure 4b reports the frequency shift, without the RF shield and for $\theta = 22.5^\circ$, calculated with D_{LP}/D_{HP} ranging from 0 (HP coil alone) to 0.93, while keeping constant $L_{LP}/L_{HP} = 0.81$. It can be seen that, as $D_{LP}/D_{HP} \rightarrow 1$, the HP frequency shift increases up to a maximum level of about 18 %, suggesting that a compromise must be set between the relative diameter of the two birdcage coils and the degree of decoupling.

Since the RF shield diameter significantly affects the coupling (Fig. 3), we have also investigated the $\Delta f/f$ dependence from the length of the RF shield. Figure 4c reports the frequency shift observed for L_S/L_{HP} ranging from 0 (no shield) to 2, while keeping constant $L_{LP}/L_{HP} = 0.65$ and $D_S/D_{HP} = 1.43$. It can be seen that $\Delta f/f$ decreases monotonically as L_S increases and, as the RF shield length equals the HP birdcage length, the frequency shift practically reaches a plateau of about 3 %, demonstrating the efficacy of the RF shield in improving decoupling.

It is interesting to consider whether the coupling between the 1H and ^{23}Na birdcage coils in the nested design, measured by means of the % frequency, shift may be field dependent. To the best of our knowledge there is no previous work dealing with this question for the nested DT birdcage RF coil design in the whole range of useful preclinical fields (2.35T-21.1T). We may give a partial answer by our additional FEM simulations of the “short” nested DT birdcage coil model performed at 2.35T, 4.7T and 7.0T. We observe that the coupling between the 1H and ^{23}Na birdcage coils, measured by means of the % frequency shift, does not varies as the field is adjusted from 2.35T to 7.0T. So, we can conclude that, within this frequency range, the coupling is practically frequency independent.

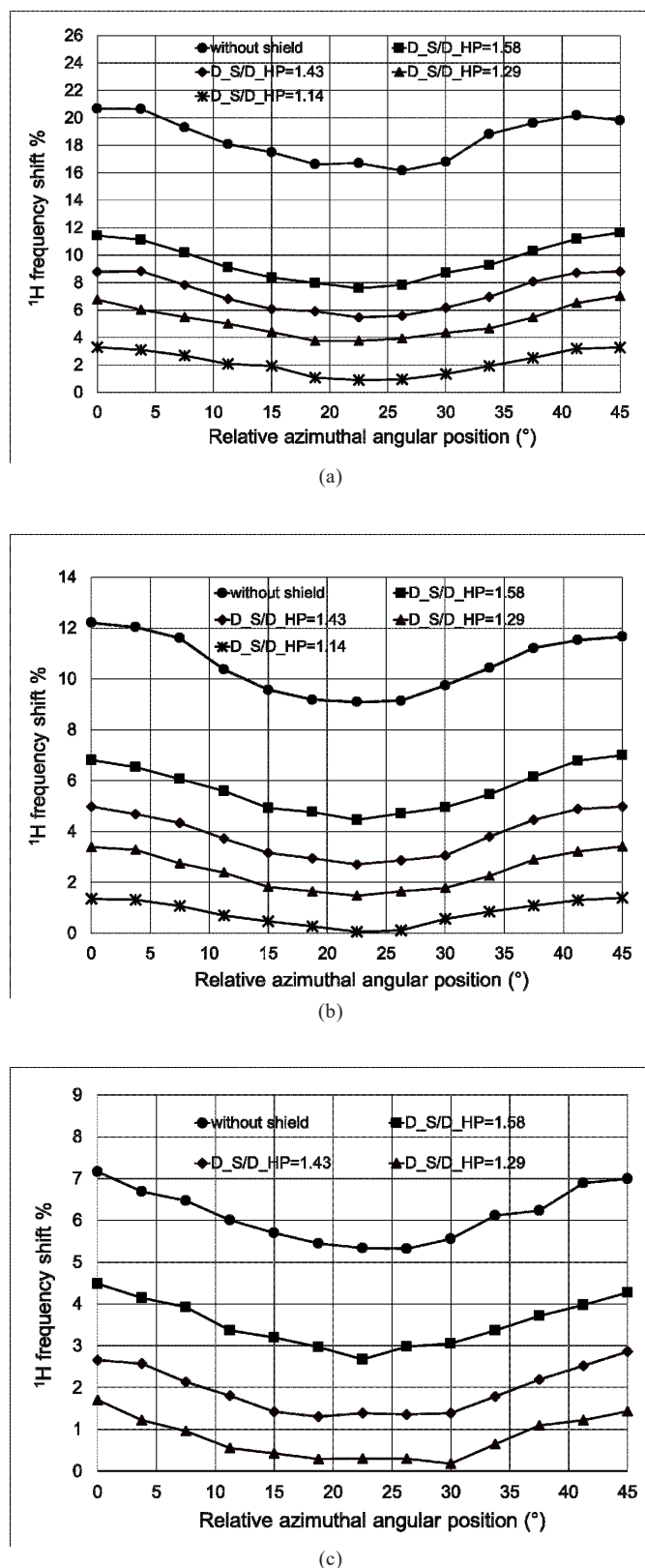


Fig. 3. Eigenmode FEM simulations of the percent frequency shift $\Delta f/f$ for the 1H useful MRI mode versus the relative azimuthal angular position without and with RF shield of various diameters ($D_{HP} = 105$ mm; $L_{HP} = 160$ mm) in the presence of the HP birdcage ($L_S/L_{HP} = 1.31$) and with: (a) the long LP birdcage RF coil ($L_{LP}/L_{HP} = 0.81$); (b) the medium LP birdcage RF coil ($L_{LP}/L_{HP} = 0.65$); and (c) the short LP birdcage RF coil ($L_{LP}/L_{HP} = 0.50$).

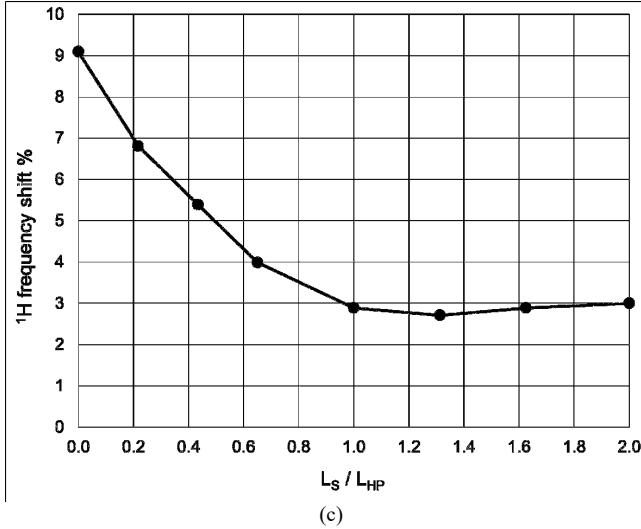
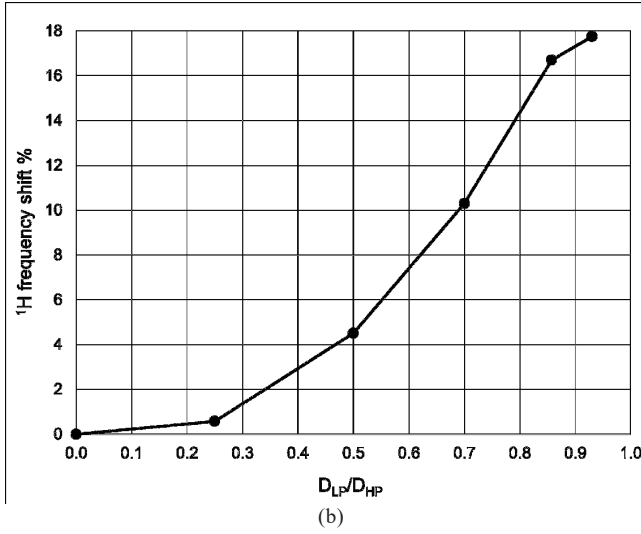
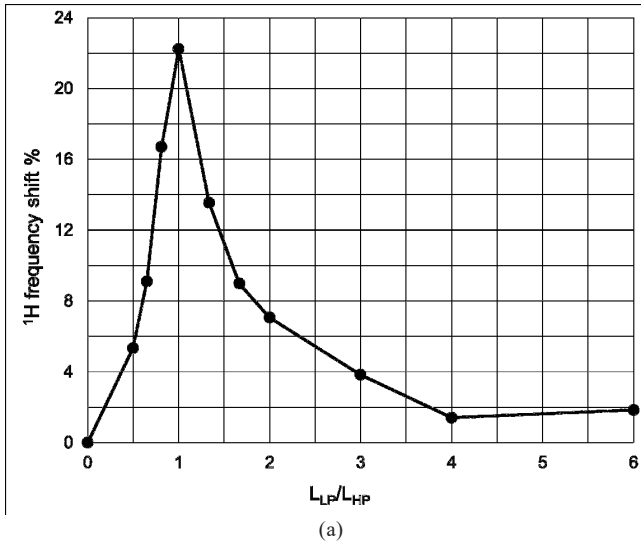


Fig. 4. Eigenmode FEM simulations of the $\Delta f/f$ for the 1H useful MRI mode of the nested HP and LP birdcage RF coils ($\theta = 22.5^\circ$): (a) without RF shield versus L_{LP}/L_{HP} ($D_{HP} = 105$ mm; $D_{LP} = 90$ mm); (b) without RF shield versus D_{LP}/D_{HP} ($L_{LP}/L_{HP} = 0.81$); and (c) with RF shield versus L_S/L_{HP} ($L_{HP} = 160$ mm; $L_{LP} = 104$ mm; $D_S = 150$ mm; $D_{HP} = 105$ mm).

B. RF B_1 Field Profiles and Coil Efficiency

As reported in textbooks [47], to better visualize the interactions between the LP and HP coils we considered only one of the two orthogonal degenerate useful MRI modes (Eigenmode FEM) to compute the modulus of the ^{23}Na and 1H transverse magnetic (B_1^+) field maps at $\theta = 22.5^\circ$. Figure 5 shows the results (in arbitrary units) for the nested HP ($L_S/L_{HP} = 1.31$) and long LP ($L_{LP} = 130$ mm; $D_S/D_{HP} = 1.14$) or short LP ($L_{LP} = 80$ mm; $D_S/D_{HP} = 1.29$) configurations in the central axial and sagittal planes.

For a better quantitative comparison Fig. 6 shows the RF B_1^+ field profiles, normalized to the value at the isocenter, along the radial and longitudinal directions for the isolated HP, isolated long LP, isolated short LP, nested HP and long LP, nested HP and short LP. All data are relative to the useful ^{23}Na and 1H modes at the critical angle of 22.5° for $D_S/D_{HP} = 1.14$ and $L_S/L_{HP} = 1.31$. From Figs. 6a and 6c it is evident that the ^{23}Na B_1^+ field profiles of the long and short LP, along the radial and longitudinal directions, are not affected by the insertion of the HP coil. On the contrary, the presence of the long or short LP has an impact on the 1H B_1^+ field profiles and, as expected, the actual length of the LP plays a relevant role. Along the radial direction the presence of the long or short LP decreases the RF field homogeneity of the HP within 80 mm of the diameter. Along the longitudinal axis both long and short LP worsen the field profile (between 20 % and 40 % variation within a 100 mm interval around the isocenter).

From our FEM simulations we have compared the unloaded Q factor of the isolated ^{23}Na and 1H RF coils versus the optimised short nested RF coil shown in Fig. 5 (c-d), considering the presence of the RF shield. We found that the unloaded Q factor of the isolated ^{23}Na and 1H RF coils are 459 and 851, respectively. In the case of the nested RF coil, the unloaded Q factor of the ^{23}Na and 1H RF coils are 436 and 811, respectively. We notice that the Q factor decreases by about 5% for both channels, a value comparable with previous designs [24]. It is worth pointing that the plots in Fig. 6 report the normalised B_1^+ distributions having taken as reference the B_1^+ value at the isocenter. However, taking into account the peak values of B_1^+ (see Table I), we observe that the absolute B_1^+ value in any spatial position of the HP alone (Fig. 6d) is higher or equal to the values of the nested HP+LP_L and HP+LP_S.

The RF coils efficiency, defined from the B_1^+ value at the isocenter, obtained from the MNA simulations, without and with RF shields (D_S/D_{HP} comprised between 1.58 and 1.04) for the ^{23}Na and 1H useful modes, are summarized in Table I. We observe that, with the short LP, the ^{23}Na channel efficiency is reduced from about 29 ($\mu T/\sqrt{W}$) (no shield) to 13 ($\mu T/\sqrt{W}$) when the smaller diameter RF shield is inserted. A slightly smaller efficiency (about 10 ($\mu T/\sqrt{W}$)) is observed for the long LP in the presence of the smaller diameter RF shield ($D_S/D_{HP} = 1.04$). The HP insertion has very little effect on the ^{23}Na efficiency, thus confirming the previous findings from the frequency shift values.

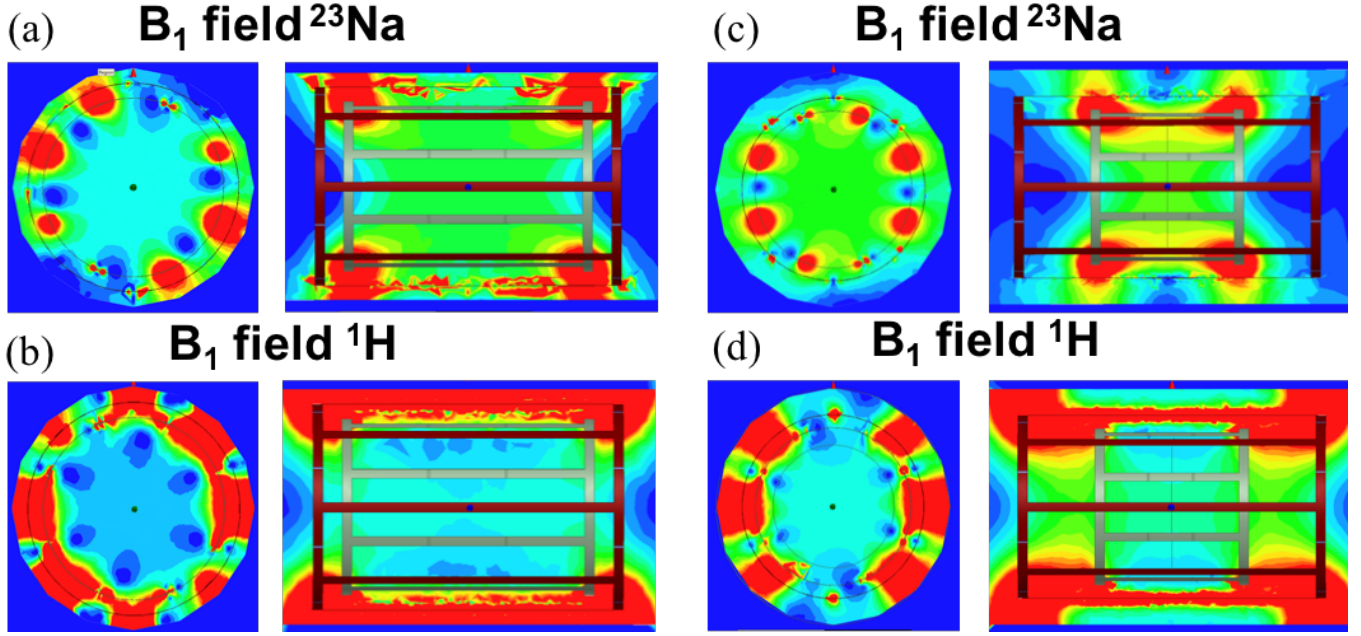


Fig. 5. Eigenmode FEM simulations: B_1^+ field maps (arbitrary units; $L_S/L_{HP} = 1.31$; $\theta = 22.5^\circ$). ^{23}Na (a, c) and ^1H (b, d) useful MRI modes in the axial (left) and sagittal (right) planes for: the nested HP ($D_S/D_{HP} = 1.14$; $D_{HP} = 105$ mm; $L_{HP} = 160$ mm) and the long LP (length 130 mm; $D_{LP} = 90$ mm); and the nested HP ($D_S/D_{HP} = 1.29$; $D_{HP} = 105$ mm; $L_{HP} = 160$ mm) and short LP (length 80 mm; $D_{LP} = 90$ mm).

The data of Table I also show that, without RF shield, increasing the LP length introduces significant reduction of the ^1H RF efficiency: from about 8 ($\mu\text{T}/\sqrt{\text{W}}$) to about 5 ($\mu\text{T}/\sqrt{\text{W}}$) for the short LP and long LP coils, respectively (to be compared with the value of about 16 ($\mu\text{T}/\sqrt{\text{W}}$) of the HP alone). We also observe that the presence of the RF shield of decreasing diameter has a large effect in reducing the HP efficiency. For example, for the short LP, the HP efficiency decreases from about 6 ($\mu\text{T}/\sqrt{\text{W}}$) to 0.8 ($\mu\text{T}/\sqrt{\text{W}}$) when the RF shield diameter ratio is reduced from 1.58 to 1.04. Similar trends are observed for the medium and long LP. The mirror currents induced on the RF shield are responsible for this efficiency decrease, and the closer distance from the shield makes the effect stronger for the HP.

The results of Table I show that the RF efficiency decreases as an RF shield is used and that such reduction increases as the shield diameter gets closer to the HP coil diameter. From the literature [48], we know that the presence of an RF shield induces some degree of increase in the resonant frequency of an isolated single-tuned RF birdcage coil, this increase being larger as the RF shield diameter is closer to the birdcage diameter. This is due to the overall decrease of the birdcage inductance due to the mutual inductive coupling between birdcage and RF shield. We may ask what degree of frequency shift is observed when an RF shield of decreasing diameter is used in the case of nested DT birdcage coils, like the one corresponding to the geometries of Table I. We will limit our analysis to the frequency variation of the ^1H HP coil, since for the ^{23}Na LP coil the frequency variation is much smaller (due to its larger distance from the shield). First, we notice that the data reported in Fig. 3 (a)-(c) for the nested birdcages (at the optimal azimuthal angle) without the presence of the RF shield (black points), show a positive increase of the ^1H frequency,

ranging from about 16 % (long LP) to 5 % (short LP). This implies that the mutual inductive coupling between the HP and LP birdcages reduces the overall inductance of the ^1H HP birdcage coil. Thus, we expect that the introduction of an RF shield of a given diameter will have a smaller effect on the resonant frequency of the nested ^1H birdcage coil with respect to the case when the ^1H coil is isolated. From our FEM simulations we verified that, in the case of the nested birdcage made by the HP and LP_L (HP and LP_S) the frequency increase of the ^1H resonant frequency related to the presence of a RF shield, is about 18 MHz (13 MHz) in the presence of an RF shield such that $D_S/D_{HP}=1.58$. Such frequency increases to 38 MHz (35 MHz) when $D_S/D_{HP}=1.04$. It is worth noting that the presence of an RF shield is a normal requirement during the coil construction and standard tools, like the Birdcage Builder

TABLE I

D_S/D_{HP}	^{23}Na				^1H			
	LP_S	HP + LP_S	LP_L	HP + LP_L	HP	HP + LP_S	HP + LP_M	HP + LP_L
Without Shield	29.2	29.3	28.4	28.2	16.3	7.7	6.3	5.2
1.58	25.5	25.2	22.9	22.9	11.1	6.3	5.3	4.4
1.43	23.6	23.7	21.0	21.0	9.5	5.6	4.8	4.0
1.29	21.3	21.0	18.2	18.2	7.2	4.6	4.0	3.4
1.14	17.2	17.1	14.1	14.1	4.1	2.8	2.6	2.2
1.06	13.6	13.5	10.8	10.7	1.5	1.3	1.1	1.0
1.04	13.0	12.8	10.1	10.1	1.1	0.8	0.7	0.7

B_1^+ ($\mu\text{T}/\sqrt{\text{W}}$) field at the isocenter from FEM MNA simulation for the isolated short LP_S , isolated long LP_L , isolated HP, nested HP and short LP_S , nested HP and medium LP_M , nested HP and long LP_L . Data are relative to the useful ^{23}Na and ^1H MRI modes considering $L_S/L_{HP} = 1.31$, $\theta = 22.5^\circ$ and a range of D_S/D_{HP} . The geometry of the LP_S , LP_L and HP RF coils were kept fixed ($D_{HP} = 105$ mm; $L_{HP} = 160$ mm; $D_{LP} = 90$ mm; length $LP_L = 130$ mm; length $LP_M = 104$ mm; length $LP_S = 80$ mm).

software, help in setting an approximate value of the capacitors. However, there are little or no guidelines to help when considering the interaction with a nested additional birdcage. For this reason, our work focused on the LP insertion effects with respect to the HP, including the RF shielded case.

C. Workbench Validation of Simulations

Figure 7 summarizes the frequency shift, from VNA measurements (symbols) and numerical FEM analysis (lines), for the nested DT RF coil prototypes in the presence of the long and short LP birdcages. The $\Delta f/f$ is measured for $0^\circ \leq \theta \leq 45^\circ$, with step $\Delta\theta = 11.25^\circ$, without and with RF shield ($D_S/D_{HP} = 1.40$, $L_S/L_{HP} = 1.31$). The $\Delta f/f$ for the ^{23}Na mode is below 1 % and it is not reported. We observe a remarkable agreement between the numerical and measured data sets, with differences within 1 % consistent with the estimated precision of the FEM simulations. Both data sets, clearly display a minimum coupling for $\theta = 22.5^\circ$. Moreover, the experimental data confirm that the coupling is strongly reduced in the presence of the RF shield and the effect depends on the LP length: about 50 % and 40 % reduction for the long and short LP, respectively.

Table II shows the theoretical and measured resonant frequencies, and the corresponding frequency shifts, for the shielded HP alone and the shielded HP in the presence of the

short LP (for $\theta = 22.5^\circ$) prototypes, both conditions without and with load (saline: $\epsilon_r = 78$; $\sigma = 1.67$ S/m). It is worth noting that as shown in Table II the tuning of the ^1H RF coil prototype was not accurate (114.44 MHz rather than 100.33 MHz). However, since we are interested in comparing the HP ^1H % frequency shift due to the interaction with the ^{23}Na LP coil, this small inaccuracy is not affecting the design guidelines reported here.

We observe that, for the shielded HP, the insertion of the load leads to a decrease of the frequency shift by about 0.2 % and 0.4 % for the short and long samples, respectively. We observe also that the LPs insertion leads to a frequency increases of about 1.4 %, as expected. Interestingly, the insertion of the short or long saline samples leads to a decrease of the resonant frequency of the nested DT RF coil, and the resultant frequency shift is less than about 0.9 %. The experimental results are in qualitative agreement with the FEM simulations and discrepancies are due to small geometrical differences between the prototypes and the FEM models.

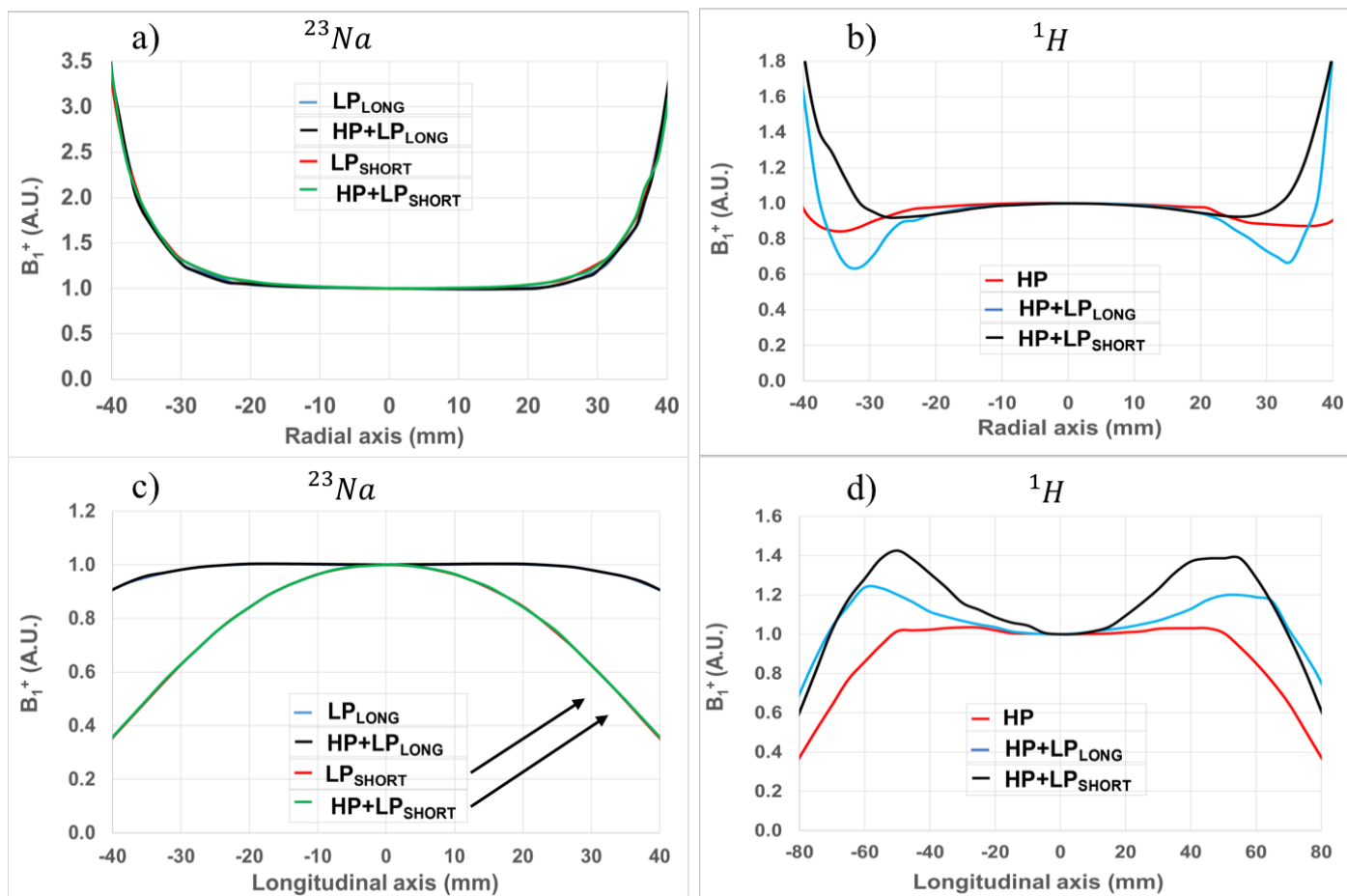


Fig. 6. Eigenmode FEM simulations: normalized B_1^+ field profiles across the birdcage RF coils isocentre along the radial (a, b) and longitudinal (c, d) directions for the isolated HP, isolated long LP, isolated short LP, nested HP and long LP, nested HP and short LP. Data are relative to the useful ^{23}Na (a, c) and ^1H (b, d) MRI modes considering: $D_S/D_{HP} = 1.14$; $L_S/L_{HP} = 1.31$; and $\theta = 22.5^\circ$. The geometry of the LPs, LP_L and HP RF coils were kept fixed ($D_{HP} = 105$ mm; $L_{HP} = 160$ mm; $D_{LP} = 90$ mm; length LP_L = 130 mm; length LP_S = 80 mm).

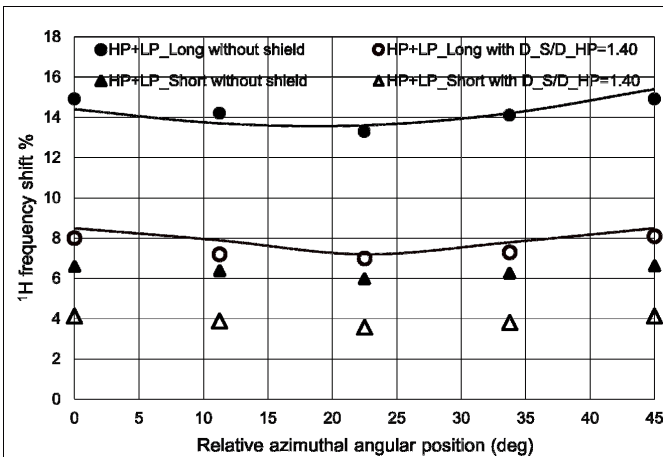


Fig. 7. Workbench measurements (symbols) and eigenmode FEM simulations (lines) of percent frequency shift $\Delta f/f$ of the ^1H useful MRI mode of the nested HP with the long (filled circles) or short (filled triangles) LP prototypes without RF shield. The corresponding data in the presence of a RF shield ($D_S/D_{HP} = 1.40$, $L_S/L_{HP} = 1.31$) are reported with open symbols.

IV. DISCUSSION

The design of the nested DT birdcage design was introduced for the first time by Fitzsimmons *et al* [24] and over the years used by several groups [25-29, 43]. It was demonstrated [24] that the performance of the nested DT coil is near optimal for the X-nuclei frequency but suffers from some degree of inefficiency in the ^1H mode due to residual coupling. However, the previous analysis did not take into account the full range of design parameter, including the presence of the RF shield. Our results show that Eigenmode FEM simulation is a useful tool to evaluate mutual coupling in nested DT birdcage RF coils, via the observable frequency shift. This approach preserves the (discrete) azimuthal rotational symmetry of the nested birdcage RF coils and also the $z \rightarrow -z$ discrete symmetry, without introducing symmetry-breaking RF driving ports necessary in the MNA FEM simulations.

The results of Figs. 3 and 7 show that the coupling between the RF coils is minimized when the legs of the LP are midway between the HP legs, i.e. at the critical angle $\theta = 360^\circ/(2N)$, assuming the same number of legs N for both birdcages. This result, already stated on a qualitative basis in the literature, has been quantified here both theoretically and experimentally for the first time. Moreover, we have shown, as from Figs. 4 and 7, that other geometrical parameters (diameter and length of the nested birdcages; RF shield diameter and length) are quite relevant for coupling optimization. For the relative length of the LP and HP birdcages, Fig. 4a shows that the maximum coupling, related to a large interaction between the end-rings, is observed for $L_{LP} = L_{HP}$, while it is strongly reduced when $L_{LP}/L_{HP} \neq 1$. Usually an LP coil shorter than the HP one is used for X-nuclei signal detection, such as to maximize the filling factor thus compensating, partially, the low X-nuclei natural abundance. Depending on the specific application, our result show that it may be useful to adopt an L_{LP}/L_{HP} less than 0.8. This suggests a clear design strategy for the nested DT RF coil: an inner LP birdcage as short as possible to cover the desired

target volume for the X-nuclei, an outer HP birdcage of larger length for ^1H imaging, since the HP can tolerate a moderate RF efficiency decrease.

The above strategy has a price to pay in terms of RF B_1^+ field homogeneity. The B_1^+ field profiles, Figs. 5 and 6, show that the ^{23}Na field is unaffected by the insertion of the HP coil, while the RF B_1^+ homogeneity of the ^1H coil is more sensitive to the presence of the LP of various lengths. We notice that the ^1H field homogeneity along the radial axis varies more in the presence of the longer LP, while the opposite behaviour is observed along the longitudinal axis. Thus, to this respect, the design strategy needs to account also the specific RF field requirements.

The FEM simulations (Figs. 4 and 5; Table I) and the experimental data (Fig. 7; Table II) demonstrate that an RF shield of suitable diameter and length is the most important component that allows to minimize and, in some condition, even to null the RF coupling. The results reported in Figs. 4, 5, 7, and Tables I, II represent a useful resource for the practical design of nested DT RF coils. However, we have also shown that the presence of the RF shield may introduce a significant reduction of the RF coil efficiency. The data of Table I demonstrate that without and with the RF shield of smaller diameter ($D_S/D_{HP} = 1.04$) the RF coil efficiency of the ^{23}Na and ^1H channels is reduced up to about 66 % and 88 %, respectively. As shown in Fig. 5, when the RF shield gets closer to the LP and HP coils, an increasing intensity of the ^1H B_1^+ field is present in between the HP and RF shield. Thus, an increasing fraction of the magnetic energy is confined in the space between the HP and the shield, while a smaller fraction of energy is stored in the central region. This turns out in a reduction of flux linkage between the nested LP and HP birdcages, hence a smaller frequency shift. The same, albeit smaller, effect is present for the ^{23}Na B_1^+ field, because of the larger ratio between the inner LP and RF shield diameters. Finally, the results reported in Fig. 4c show that when $L_S \geq L_{HP}$, the frequency shift is minimized. This is a typically required condition to guarantee also good isolation from close-by conductive structures.

The results and design guidelines presented in this work were obtained for the nested $^{23}\text{Na}/^1\text{H}$ numerical models and prototypes suitable for 2.35T preclinical scanners. However, they should remain qualitatively similar if the LP birdcage is tuned at frequencies other than ^{23}Na , with the condition that the LP resonant frequencies are far away from the HP resonant modes. In the most conservative approach, this happens when the higher resonant frequency (f_{LP4}) of the LP gets very close to the lowest resonant frequency (f_{HP4}) of the HP. The full bandwidth of the LP ($BW_{LP} = f_{LP4} - f_{LP1}$) and HP ($BW_{HP} = f_{HP1} - f_{HP4}$) RF coils are determined by the respective geometries (legs number; coil diameter and length). At 2.35T and with our geometrical conditions (8 legs; ^{23}Na diameter 90 mm and length 130 mm; ^1H diameter 105 mm and length 160 mm) we have $BW_{LP} = 18$ MHz and $BW_{HP} = 37$ MHz. Those values set the limit of the useful X-nuclei resonant frequency to be about 45 MHz having considered the ^1H nuclei as the other desired nuclei of the DT nested coil. The analysis of the most used X-nuclei for

biomedical applications shows that all X-nuclei can be observed, except ^{19}F and ^3He . This makes the nested design described here of general use.

It is interesting to consider whether it may be possible applying the quantitative numerical and workbench findings obtained at 2.35T to a wider range of UHF preclinical MRI scanners (3.0T, 4.7T, 7.0T, 9.4T, 11.7T, 15.2T, 21.1T) and possibly also to clinical (3.0T, 7.0T, 9.4T, 10.5T) MRI systems. First, we notice that the 2.35T preclinical findings are already applicable to the novel class of low-cost preclinical bench 3.0T MRI commercial systems (Bruker Biospec; MRSolutions Ltd) suitable for rats and mice applications, and also for combined 3.0T preclinical MRI/PET studies. In fact, we do not expect significant design changes as the operating frequencies shift from about 100/27 MHz ($^1\text{H}/^{23}\text{Na}$ at 2.35T) to 128/34 MHz ($^1\text{H}/^{23}\text{Na}$ at 3.0T). So, we believe our results are useful for an expanding community of researchers working on preclinical 3.0T bench MRI systems. To further develop on this specific point, we have performed a full FEM simulation of the nested DT RF coil design with the short LP birdcage at higher frequencies, such as to verify the ability to work at UHF, leaving the geometrical parameters unchanged. This goal seems feasible from a practical point of view, since the current tuning capacitors for the 2.35T ^1H birdcage coil are about 53 pF (tuning about 100 MHz). By reducing the ^1H tuning capacitors to about 12 pF or 5 pF (feasible values in practical conditions) the resonant frequency shifts to about 200 MHz or 298 MHz, allowing operation of the ^1H birdcage at 4.7T or 7.0T, respectively. Our FEM simulations show that at 4.7T and 7.0T the ^1H frequency shift remains below 1 %, thus confirming that the current nested DT RF coil design is suitable for MRI systems operating up to 7.0T. The use at higher fields would require some degree of adjustment of the nested DT RF coil geometry, with the aim to reduce the overall inductance of the ^1H HP birdcage. Accurate designs for the LP and HP birdcages are reported in the literature for the single tuned birdcage coil [46] and could be adapted for the current DT nested configuration. Finally, an interesting question is related to the translation value of the 2.35T preclinical findings with respect to clinical UHF MRI systems (3.0T, 7.0T, 9.4T, 10.5T). We believe it may be relatively straightforward to adapt our 2.35T design guidelines to the specific case of 3.0T MRI scanner used for human head applications. As before, we do not expect significant design changes as the operating field shifts from 2.35T to 3.0T. Rather, we are aware that the main critical issues would be the self and mutual inductance of the nested RF birdcages coils as we scale up the coil diameters, say from our reported size of 7 cm (rats) to about 16 cm (human head) or 70 cm (whole-body). In this case we should also consider the necessary increase of the number of birdcage coil's elements (rungs) necessary to maintain a good transverse RF field homogeneity and also additional coupling effects due to presence of the loading sample [49]. However, a full description of the optimized design for clinical UHF (7.0-10.5T) MRI systems is beyond the aims of this current work. A preliminary account of 7.0T human head nested RF birdcage coils has been reported elsewhere [50-51]. An alternative design suitable for

7.0T human head applications using the four-ring birdcage coil geometry has also been recently reported [51].

TABLE II

^1H	HP	HP + Long sample or Short sample	HP + short LP	HP+ short LP + Long sample or Short sample
f_0 (MHz) FEM	99.86	99.67 99.47	101.25	100.79 100.72
$\Delta f/f$ (%) FEM	-	-0.19 % -0.39 %	1.40 %	0.93 % 0.86 %
f_0 (MHz) Meas.	114.44	114.34 114.08	117.57	117.57 117.20
$\Delta f/f$ (%) Meas.	-	-0.09 % -0.32 %	2.73 %	2.73 % 2.41 %

Simulated (FEM Eigenmode) and experimental dependence of the resonant frequency ($\theta = 22.5^\circ$ for the nested configurations) of the shielded RF coils in the presence of a physiological saline samples ($\epsilon_r = 78$; $\sigma = 1.67$ S/m). FEM model has: short LP (length 80 mm; diameter 90 mm; strip width 5 mm); HP (length 160 mm; diameter 105 mm; strip width 5 mm); RF shield (length 210 mm; diameter 150 mm); and sample (diameter 80 mm; short length 80 mm; long length 210 mm). The experimental prototype has: short LP (length 80 mm; diameter 75 mm; strip width 6 mm); HP (length 160 mm; diameter 100 mm; strip width 13 mm); RF shield (length 210 mm; diameter 140 mm) and sample (diameter 59 mm; short length 80 mm; long length 210 mm).

One of the main drawbacks of the nested DT birdcage configuration, despite its conceptual simplicity and easy construction, is the small residual HP frequency shift due to non-compensated RF coupling in the presence of the loading sample. This effect can be corrected with a fine-tuning of the HP birdcage with respect to the isolated configuration. However, the large number of capacitors used for the HP birdcage realization makes this procedure cumbersome, unless the residual frequency shift is small (less than few %) and can be compensated acting on a single tuning capacitor.

V. CONCLUSIONS

This work presents, for the first time, a detailed analysis of nested DT birdcage RF coil configurations. Workbench tests have been performed to confirm the accuracy of the numerical FEM simulations such as to provide evidence of coupling minimization with respect to: (i) azimuthal angular orientation; (ii) length and diameter of the birdcage coils; and (iii) length and diameter of the RF shield. FEM simulations were used to expand the results to a large range of geometrical configurations, so to give quantitative guidelines to the RF coil designers. We have shown that in favourable geometrical conditions the use of a RF shield is able to null the mutual coupling between the ^{23}Na and ^1H birdcages.

However, we have shown that this optimal decoupling condition comes with a price to pay, i.e. the decreased ^1H RF B_1^+ efficiency. We have provided extensive guidelines on how to set a reasonable compromise between improved isolation and decreased efficiency, and for each specific application it will be necessary to evaluate which one is to be considered as prominent. It is worth mentioning that ^1H traps could be placed into each, or some, of the ^{23}Na RF coil legs such as to reduce coupling, as suggested in past work for surface RF coils [8].

This could somehow release the condition about the close-fitting RF shield diameter, with an advantage in terms of improved RF efficiency. Future work will be necessary to explore this interesting option.

In conclusion, RF coils design is often a tricky optimization process where trade-off between RF homogeneity, RF efficiency and practical constraints occurs. In the case of the nested DT design presented here, we demonstrated that the relative angular position could be optimized to reduce coupling without adverse effects. The other geometrical parameters studied here (RF coil length, shield diameter and length) also affect the RF coupling, the homogeneity and the efficiency. We have reported extensive guidelines to select the best solution depending on the specific application. The indications provided here should help and speed-up the design process of nested DT RF coils, avoiding pitfalls and pursuing the best conditions. The results presented here were obtained for $^1\text{H}/^{23}\text{Na}$ prototypes suitable for a 2.35 T preclinical scanner. However, the presented design guidelines can be easily adapted to other X nuclei, coil sizes and operating frequencies.

VI. ACKNOWLEDGMENTS

We thank Dr. Assunta Vitacolonna for her help with preliminary modeling. The Referees are kindly acknowledged for their constructive comments and suggestions.

REFERENCES

- [1] I. K. Steinseifer, J. P. Wijnen, B. C. Hamans, A. Heerschap, T. W. J. Scheenen, "Metabolic imaging of multiple X-nucleus resonances", *Magn. Reson. Med.*, vol. 70, pp. 169–175, July 2013.
- [2] K. Ugurbil, "Magnetic Resonance Imaging at Ultrahigh Fields", *IEEE Trans. Biomed. Eng.*, vol. 61, no. 5, pp. 1364–1379, May 2014.
- [3] M. D. Schnall, V. Hariharasubramanian, J. S. Leigh, B. Chance, "A new double-tuned probe for concurrent ^1H and ^{31}P NMR", *J. Magn. Reson.*, vol. 65, no. 1, pp. 122–129, Oct. 1985.
- [4] C. H. Choi, Y. Ha, P. Veeraiha, J. Felder, K. Möllenhoff, N. J. Shah, "Design and implementation of a simple multinuclear MRI system for ultra high-field imaging of animals", *J. Magn. Reson.*, vol. 273, pp. 28–32, Dec. 2016.
- [5] C. H. Choi, S. M. Hong, Y. Ha, N. J. Shah, "Design and construction of a novel $^1\text{H}/^{19}\text{F}$ double-tuned coil system using PIN-diode switches at 9.4 T", *J. Magn. Reson.*, vol. 279, pp. 11–15, June 2017.
- [6] Y. Ha, C. H. Choi, N. J. Shah, "Development and implementation of a PIN-diode controlled, quadrature-enhanced, double-tuned RF coil for sodium MRI", *IEEE Trans. Med. Imaging*, vol. 37, no. 7, pp. 1626–1631, July 2018.
- [7] J. R. Fitzsimmons, H. R. Brooker, B. Beck, "A transformer-coupled double-resonant probe for NMR imaging and spectroscopy", *Magn. Reson. Med.*, vol. 5, no. 5, pp. 471–477, Nov. 1987.
- [8] M. Alecci, S. Romanzetti, J. Kaffanke, A. Celik, H. P. Wegener, N. J. Shah, "Practical design of a 4 Tesla double-tuned RF surface coil for interleaved ^1H and ^{23}Na MRI of rat brain", *J. Magn. Reson.*, vol. 181, no. 2, pp. 203–211, Aug. 2006.
- [9] Y. Pang, X. Zhang, Z. Xie, C. Wang, D. B. Vigneron, "Common-mode differential-mode (CMDM) method for double-nuclear MR signal excitation and reception at ultrahigh fields", *IEEE Trans. Med. Imaging*, vol. 30, no. 11, pp. 1965–1973, Nov. 2011.
- [10] F. Wetterling, M. Högl, U. Molkenthin, S. Junge, L. Gallagher, I. Mhairi MacRae, A. J. Fagan, "The design of a double-tuned two-port surface resonator and its application to in vivo Hydrogen- and Sodium-MRI", *J. Magn. Reson.*, vol. 217, pp. 10–18, Apr. 2012.
- [11] P. Cao, X. Zhang, I. Park, C. Najac, S. J. Nelson, S. Ronen, P. E. Z. Larson, " ^{13}C independently tuned radiofrequency surface coil applied for in vivo hyperpolarized MRI", *Magn. Reson. Med.*, vol. 76, no. 5, pp. 1612–1620, Nov. 2016.
- [12] N. I. Avdievich, "Transceiver-Phased Arrays for Human Brain Studies at 7 T", *Appl. Magn. Reson.*, vol. 41, no. 2–4, pp. 483–506, Dec. 2011.
- [13] M. D. Wilcox, R. Del Bosque, K. Parizek, J. Sia, E. D. Eigenbrodt, M. P. McDougall, "A three-element $^1\text{H}/^{31}\text{P}$ dual-tuned array for magnetic resonance spectroscopy at 4.7 T", in *38th Annu. Int. Conf. IEEE Eng. Med. Biol. Soc.*, Orlando, Florida USA, 2016, pp. 6258–6261.
- [14] G. Isaac, M. D. Schnall, R. E. Lenkinski, K. Voegelé, "A design for a double-tuned birdcage coil for use in an integrated MRI/MRS examination", *J. Magn. Reson.*, vol. 89, no. 1, pp. 41–50, Aug. 1990.
- [15] A. R. Rath, "Design and performance of a double-tuned bird-cage coil", *J. Magn. Reson.*, vol. 86, no. 3, pp. 488–495, Feb. 1990.
- [16] J. Murphy-Boesch, R. Srinivasan, L. Carvajal, T. R. Brown, "Two configurations of the four-ring birdcage coil for ^1H imaging and ^1H -decoupled ^{31}P spectroscopy of the human head", *J. Magn. Reson. B.*, vol. 103, no. 2, pp. 103–114, Feb. 1994.
- [17] J. T. Vaughan, H. P. Hetherington, J. O. Otu, J. W. Pan, G. M. Pohost, "High frequency volume coils for clinical NMR imaging and spectroscopy", *Magn. Reson. Med.*, vol. 32, no. 2, pp. 206–218, Aug. 1994.
- [18] G. X. Shen, F. E. Boada, K. R. Thulborn, "Dual-frequency, dual-quadrature, birdcage RF coil design with identical B1 pattern for sodium and proton imaging of the human brain at 1.5 T", *Magn. Reson. Med.*, vol. 38, no. 5, pp. 717–725, Nov. 1997.
- [19] G. B. Matson, P. Vermathen, T. C. Hill, "A practical double-tuned $^1\text{H}/^{31}\text{P}$ quadrature birdcage headcoil optimized for ^{31}P operation", *Magn. Reson. Med.*, vol. 42, no. 1, pp. 173–182, July 1999.
- [20] T. Lanz, J. Ruff, A. Weisser, A. Haase, "Double tuned ^{23}Na ^1H nuclear magnetic resonance birdcage for application on mice in vivo", *Rev. Sci. Instrum.*, vol. 72, no. 5, pp. 2508–2510, May 2001.
- [21] A. Vitacolonna, G. Placidi, A. Sotgiu, P. Jezzard, M. Alecci, "Theory of Double Tuned TEM Resonators and Workbench Validation in a Frequency Range of 100–350 MHz", in *13th SMRM*, Miami, Florida USA, 2005, p. 2423.
- [22] N. I. Avdievich, H. P. Hetherington, "4 T Actively-detuneable double-tuned $^1\text{H}/^{31}\text{P}$ head volume coil and four-channel ^{31}P phased array for human brain spectroscopy", *J. Magn. Reson.*, vol. 186, no. 2, pp. 341–346, Mar. 2007.
- [23] S. M. Hong, C. H. Choi, A. W. Magill, N. J. Shah, J. Felder, "Design of a quadrature $^1\text{H}/^{31}\text{P}$ coil using bend dipole antenna and 4-channel loop at 3T MRI", *IEEE Trans. Med. Imaging*, DOI: 10.1109/TMI.2018.2844462, 6 June 2018.
- [24] J. R. Fitzsimmons, B. Beck, H. R. Brooker, "Double resonant quadrature birdcage", *Magn. Reson. Med.*, vol. 30, no. 1, pp. 107–114, July 1993.
- [25] A. Asfour, "A three-coil RF probe-head at 2.35 T: Potential applications to the ^{23}Na and to the hyperpolarized ^{129}Xe MRI in small animals", in *Ann. Int. Conf. IEEE Eng. Med. Biol. Soc.*, Buenos Aires, Arg., 2010, pp. 5693–5699.
- [26] R. C. Brand, A. G. Webb, J.-W. M. Beenakker, "Design and performance of a transformer-coupled double resonant quadrature birdcage coil for localized proton and phosphorus spectroscopy in the human calf muscle at 7 T", *Concepts Magn. Reson. Part A*, vol. 42, no. 5, pp. 155–164, Sept. 2013.
- [27] G. Giovannetti, G. Valvano, G. Virgili, M. Giannoni, A. Flori, F. Frijia, D. De Marchi, V. Hartwig, L. Landini, G. D. Aquaro, A. Pingitore, "Design and simulation of a dual-tuned $^1\text{H}/^{23}\text{Na}$ birdcage coil for MRS studies in human calf", *Appl. Magn. Reson.*, vol. 46, no. 11, pp. 1221–1238, Nov. 2015.
- [28] A. Vitacolonna, A. Galante, T. M. Florio, A. Chincari, A. Retico, M. Alecci, "Simulation, Development and Workbench Testing of a Double-Tuned ($^{23}\text{Na}/^1\text{H}$) Nested Birdcage RF Coil for MRI Application", in *102th Meeting of the Italian Physical Society*, Padua, Italy, 2016, p. 128.
- [29] A. Galante, M. Fantasia, M. Alecci, "Optimization study of a double-tuned nested birdcage RF coil for $^1\text{H}/^{23}\text{Na}$ MRI", *Proc. Intl. Soc. Mag. Reson. Med.*, vol. 26, pp. 1719, May 2018.
- [30] Y. Ha, C. H. Choi, W. A. Worthoff, A. Shymanskaya, M. Schöneck, A. Willuweit, J. Felder, N. J. Shah, "Design and use of a folded four-ring double-tuned birdcage coil for rat brain sodium imaging at 9.4 T", *J. Magn. Reson.*, vol. 286, pp. 110–114, Jan. 2018.
- [31] F. E. Terman, Radio Engineering, McGraw-Hill, New York, 1937.
- [32] N. Gurler, Y. Z. Ider, "FEM based Design and Simulation Tool for MRI Birdcage Coils including Eigenfrequency Analysis", in *COMSOL Conf.*, Milan, Italy, 2012.
- [33] M. Kozlov, R. Turner, "Fast MRI coil analysis based on 3-D electromagnetic and RF circuit co-simulation", *J. Magn. Reson.*, vol. 200, pp. 147–152, Sept. 2009.

- [34] S. K. Hilal, A. A. Maudsley, H. E. Simon, W. H. Perman, J. Bonn, M. E. Mawad, A. J. Silver, S. R. Ganti, P. Sane, I. C. Chien, "In vivo NMR imaging of tissue sodium in the intact cat before and after acute cerebral stroke", *Am. J. Neuroradiol.*, vol. 4, no. 3, pp. 245–249, May 1983.
- [35] R. Ouwerkerk, K. B. Bleich, J. S. Gillen, M. G. Pomper, P. A. Bottomley, "Tissue sodium concentration in human brain tumors as measured with ^{23}Na MR Imaging", *Radiology*, vol. 227, no. 2, pp. 529–537, May 2003.
- [36] V. D. Schepkin, B. D. Ross, T. L. Chenevert, A. Rehemtulla, S. Sharma, M. Kumar, J. Stojanovska, "Sodium magnetic resonance imaging of chemotherapeutic response in a rat glioma", *Magn. Reson. Med.*, vol. 53, no. 1, pp. 85–92, Jan. 2005.
- [37] A. Borthakur, E. Mellon, S. Niyogi, W. Witschey, J. B. Kneeland, R. Reddy, "Sodium and T1rho MRI for molecular and diagnostic imaging of articular cartilage", *NMR Biomed.*, vol. 19, no. 7, pp. 718–821, Nov. 2006.
- [38] N. Maril, Y. Rosen, G. H. Reynolds, A. Ivanishev, L. Ngo, R. E. Lenkinski, "Sodium MRI of the human kidney at 3 Tesla", *Magn. Reson. Med.*, vol. 56, no 6, pp. 1229–1234, Dec. 2006.
- [39] B. S. Solanky, F. Riemer, X. Golay, C. A. Wheeler-Kingshott, "Sodium quantification in the spinal cord at 3T", *Magn Reson Med.*, vol. 69, no. 5, pp. 1201–1208, May 2013.
- [40] G. Madelin, J. S. Lee, R. R. Regatte, A. Jerschow, "Sodium MRI: Methods and applications", *Prog. Nucl. Magn. Reson. Spectrosc.*, vol. 79, pp. 14–47, May 2014.
- [41] S. Konstandin, L. R. Schad, "30 Years of sodium/X-nuclei magnetic resonance imaging", *Magn. Reson. Mater. Phys.*, vol. 27, no. 1, pp. 1–4, Feb. 2014.
- [42] N. J. Shah, W. A. Worthoff, K. J. Langen, "Imaging of sodium in the brain: a brief review", *NMR Biomed.*, vol. 29, no. 2, pp. 162–174, Feb. 2016.
- [43] A.M. Hudson, W. Köckenberger, R.W. Bowtell, "Dual resonant birdcage coils for ^1H detected ^{13}C microscopic imaging at 11.7 T", *Magn. Reson. Mater. Phys.*, vol. 10, pp. 61–68, June 2000.
- [44] S. Mookherjea, "Spectral characteristics of coupled resonators", *J. Opt. Soc. Am. B*, vol. 23, no. 6, pp. 1137, June 2006.
- [45] V. Tyurnev, "Coupling coefficients of resonators in microwave filter theory", *Prog. Electromagn. Res. B*, vol. 21, pp. 47–67, Jan. 2010.
- [46] J. Mispelter, M. Lupu, and A. Briguet, "NMR Probeheads for Biophysical and Biomedical Experiments. Theoretical Principles and Practical Guidelines", 2nd ed., Imperial College Press, 2015.
- [47] A.G. Webb, "Magnetic Resonance Technology. Hardware and System Components Design", The Royal Society of Chemistry, 2016.
- [48] J. Jin, "Electromagnetic analysis and design in MRI", CRC Press, 1999.
- [49] M. Alecci, C. M. Collins, M. B. Smith, P. Jezzard, "Radio frequency magnetic field mapping of a 3 Tesla birdcage coil: experimental and theoretical dependence on sample properties", *Magn. Reson. Med.*, vol. 46, pp. 379–385, July 2001.
- [50] F. Maggiorelli, "Design and Development of Radio Frequency Coils for Sodium Magnetic Resonance Imaging at 7 T", PhD Thesis, University of Siena, Italy, 2019.
- [51] F. Maggiorelli, A. Retico, E. Boskamp, F. Robb, A. Galante, M. Fantasia, M. Alecci, M. Tosetti, G. Tiberi, "Double Tuned ^1H - ^{23}Na Birdcage Coils for MRI at 7T. Performance evaluation through electromagnetic simulations", *Proc. IEEE International Symposium on Medical Measurements and Applications (MeMeA)*, pp. 129–134, Aug. 2018.